CrossMark
click for updates

Virtual screening campaigns and ADMET evaluation to unlock the potency of flavonoids from Erythrina as 3CLpro SARS-COV-2 inhibitors

Vicki Nishinarizki[1] iD, Ari Hardianto[1] iD, Shabarni Gaffar[1] iD, Muchtaridi Muchtaridi[2] iD, Tati Herlina[1*] iD

[1]Department of Chemistry, Faculty of Mathematics and Natural Sciences, Universitas Padjadjaran, Jatinangor, Indonesia.
[2]Faculty of Pharmacy, Universitas Padjadjaran, Jatinangor, Indonesia.

ARTICLE INFO

ABSTRACT

Severe acute respiratory syndrome coronavirus 2 (SARS-CoV-2) has caused the coronavirus disease 2019 (COVID-19) pandemic with more than 6 million deaths worldwide. Flavonoids from the genus *Erythrina* may inhibit SARS-CoV-2, targeting 3C-like protease (3CLpro), an enzyme essential in the virus's growth. Hence, this study aimed to screen 378 flavonoids from *Erythrina* against 3CLpro, using molecular docking, Lipinski's rule of five, and *in silico* absorption, distribution, metabolism, excretion, and toxicity. These virtual screening campaigns suggest that 108 flavonoids have stronger binding energy values (−13.23 to −10.20 kcal/mol) than the N3 inhibitor (−10.14 kcal/mol) as the reference ligand. Some 33 of these flavonoids may be hepatoxicity- and mutagenicity-free. They are also non-hERG I and II inhibitors. Two of them, orientanol E (**171**) and erycaffra F (**57**), have binding energy values in the top 10 hits and good absorption profiles, despite their poor distribution properties. They may have a high bioavailability in the body and be excreted from the body through feces. Conducted molecular dynamics simulations also support orientanol E (**171**) and erycaffra F (**57**) as 3CLpro inhibitor candidates. Our study suggests that flavonoids from *Erythrina* have potential as 3CLpro inhibitors, which help guide further *in vitro* and *in vivo* experiments in COVID-19 drug development.

INTRODUCTION

The coronavirus disease 2019 (COVID-19) pandemic has burdened countries worldwide since early 2020. By mid-2022, COVID-19 cases had reached 564,266,029 and caused more than 6 million deaths (Worldometers, 2022). It is caused by severe acute respiratory syndrome coronavirus 2 (SARS-CoV-2), attacking some organs, particularly the lungs (Morse *et al.*, 2020).

SARS-CoV-2 belongs to the subfamily Orthocoronavirinae in the family Coronaviridae and order Nidovirales (Cui *et al.*, 2019). It is an enveloped positive-stranded RNA (+ssRNA) virus with a genome size of 26–32 kb coding structural and non-structural proteins (nsp1-16) (Gil *et al.*, 2020; Ji *et al.*, 2020; Mody *et al.*, 2021). Among these proteins, 3C-like protease (3CLpro) has been reported to be essential for controlling the multiplication cycle of SARS-CoV-2 (Mody *et al.*, 2021; Petrou *et al.*, 2022; Zhu *et al.*, 2022). It cleaves polyproteins 1ab at 11 sites into mature functional proteins (nsp5-16) (Lee *et al.*, 2020). Based on cleavage sequence variation, 3CLpro presents in all genera of coronaviruses, such as *Alpha-*, *Beta-*, *Gamma-*, and *Deltacoronavirus* (Kiemer *et al.*, 2004; Prescott, 2022). Therefore, inhibition on 3CLpro may halt the spread of coronavirus infections, especially SARS-CoV-2.

Several studies have suggested that natural products can inhibit 3CLpro (Liu *et al.*, 2021; Su *et al.*, 2021). Myricetin exhibits IC_{50} of 0.30 μM to 3CLpro by interacting with the catalytic site residues (Cys145 and His41) (Su *et al.*, 2021). Meanwhile, baicalein shows a potent inhibitory activity to 3CLpro with IC_{50} of 0.39 μM (Liu *et al.*, 2021). Both flavonoids have high inhibition

*Corresponding Author
Tati Herlina, Department of Chemistry, Faculty of Mathematics and Natural
Sciences, Universitas Padjadjaran, Sumedang, Indonesia.
E-mail: tati.herlina @ unpad.ac.id

activities since their IC$_{50}$ values are below 20 μM (Liu *et al.*, 2008) and shed light on the potency of other flavonoids as 3CL^{pro} inhibitors.

Another source of flavonoids is the genus *Erythrina*, which is grown in tropical and subtropical regions, including Indonesia (Fahmy *et al.*, 2018; Herlina *et al.*, 2011). Some 378 flavonoids have been isolated from *Erythrina* plants. They are flavones, flavonols, flavanones, chalcones, isoflavans, isoflav-3-enes, isoflavanones, isoflavones, pterocarpans, 6α-hydroxypterocarpans, pterocarpenes, coumestans, 3-arylcoumarins, coumaronochromones, 2-arylbenzofurans, 3-aryl-2,3-dihydrobenzofurans, and biflavonoids. Lee *et al.* (2009) demonstrated that alpinumisoflavone from the genus *Erythrina* potentially inhibits the growth of human immunodeficiency virus type 1. Furthermore, vitexin isolated from the genus *Erythrina* potentially inhibits the expression of DNA in herpes simplex virus type 1 (Fahmy *et al.*, 2020). Nonetheless, despite their potencies, flavonoids from *Erythrina* have not been investigated for their inhibition activities to SARS-CoV-2, especially targeting 3CL^{pro}. Hence, the study on flavonoids from *Erythrina* as 3CL^{pro} inhibitors is vital in the development of anti-SARS-CoV-2 agents.

Nowadays, *in silico* approaches are the most commonly used methods to accelerate drug discovery from natural products (Ramírez and Caballero, 2018). One of them is molecular docking, which has been utilized in various studies (Hardianto *et al.*, 2021; Petrou *et al.*, 2022; Raschi *et al.*, 2009; Ul Qamar *et al.*, 2017). Molecular docking has assisted Yamamoto *et al.* (2022) in virtually screening 3CL^{pro} inhibitors from the Enamine library before *in vitro* assays. It was also used by Ahmad *et al.* (2021) as one of the methods to elucidate the molecular mechanism of PF-07321332, an oral drug for COVID-19 treatment, in inhibiting 3CL^{pro}. Therefore, we used molecular docking to screen 378 flavonoids from *Erythrina* as 3CL^{pro} potential inhibitors. Meanwhile, to evaluate the drug-likeness of the screened flavonoids as orally active drugs, we employed Lipinski's rule of five (Ro5) (Lipinski *et al.*, 2012). We also performed molecular dynamics (MD) simulations to top hits for more realistic energy prediction (Forli *et al.*, 2016).

Another vital aspect of drug development is the absorption, distribution, metabolism, excretion, and toxicity (ADMET) of compounds in the body. Absorption, distribution, metabolism, and excretion (ADME) data provide information to assess drug molecule candidates in crossing the small intestine, which eventually are distributed to target cells, metabolized, and cleared from the human body. Metabolism is an important process in activating some drug molecules. However, it may also convert drug molecules into toxic forms (Daina *et al.*, 2017; Gil *et al.*, 2020; Kavaliauskas *et al.*, 2020). Hence, we evaluate the ADMET properties of flavonoids from *Erythrina* using an *in silico* approach via the pkCSM web server (Pires *et al.*, 2015). Our study suggests that flavonoids from *Erythrina* have potential as 3CL^{pro} inhibitors, which help guide further *in vitro* and *in vivo* experiments in COVID-19 drug development.

MATERIALS AND METHODS

Flavonoid structures preparation

Fahmy *et al.* (2018) reported that 378 flavonoids have been isolated from the genus *Erythrina*. The two-dimensional (2D) structures of the flavonoids were sketched in Chemaxon MarvinSketch (Chemaxon, 2020). The protonated states of the flavonoids at physiological pH (7.4) were predicted using the same program, Chemaxon MarvinSketch. Their three-dimensional (3D) structures with the protonated states at physiological pH were saved in .pdb format. MGLTools 1.5.6 (Forli *et al.*, 2016) was utilized to prepare the 3D structures for molecular docking.

Molecular docking validation

The crystal structure of 3CL^{pro} was retrieved from the Protein Data Bank (PDB) website (https://www.rcsb.org) with PDB ID 6LU7 (Jin *et al.*, 2020). The 3D structures of 3CL^{pro} and its inhibitor (N3) (Saur *et al.*, 2021; Yang *et al.*, 2005) were separated in BIOVIA Discovery Studio (DS) 2020 Client and saved as separated pdb files, while the water and ion molecules were discarded. Subsequently, both structures were subjected to AutoDockTools 1.5.6 for the preparation of molecular docking validation. Nonpolar hydrogen atoms were removed, whereas the polar ones were retained. The Gasteiger and Kollman atomic charges (Forli *et al.*, 2016) were added to the N3 and 3CL^{pro} structures, respectively. The active torsions of the N3 structure were set as suggested by AutoDockTools 1.5.6. Both 3CL^{pro} and N3 structures were saved as a pdbqt format. The dimension of the grid box was set to cover the whole structure of N3. Grid maps at the binding site of 3CL^{pro} were computed using the AutoGrid4.2 program. A Lamarckian genetic algorithm (GA) was selected in molecular docking. The number of GA runs and population size were set to 100 and 300, respectively. Meanwhile, the maximum number of evaluations was 2.500.000 times (medium). The rest of the search parameters were set to defaults, and so were docking parameters. Molecular docking validation was performed by redocking the N3 structure to the binding site of 3CL^{pro}. The validation step was considered a success if the root mean square deviation (RMSD) of the docked N3 was below 2.00 Å (Gohlke *et al.*, 2000; Kissler *et al.*, 2020).

Virtual screening campaigns

The preparation of flavonoid structures in AutoDockTools 1.5.6 followed the steps in the molecular docking validation above. We performed virtual screening campaigns using Raccoon v1.0b on an Ubuntu 20.04 operating system. The grid map and docking parameters used in molecular docking validation were employed as templates. The virtual screening results were analyzed in AutoDockTools 1.5.6.

Lipinski's Ro5 calculation

Hits from virtual screening campaigns were subjected to Lipinski's Ro5 (Cheng *et al.*, 2012; Lipinski *et al.*, 2012) in the SwissADME (http://www.swissadme.ch/) web server. This step was to assess the potency of hits as orally active drug candidates. Lipinski's Ro5 evaluates hits based on their molecular weights (MWs), logP values, and hydrogen bond donors (HBDs) and acceptors (HBAs).

ADMET prediction

ADMET prediction was conducted through the pkCSM web server (http://biosig.unimelb.edu.au/pkcsm). The absorption criteria consist of water solubility, Caco2 permeability, human intestinal absorption, P-glycoprotein substrate, and P-glycoprotein I and II inhibitors. Hit distribution prediction involves the steady-

state volume of distribution (VDss), fraction unbound, blood–brain barrier (BBB), and central nervous system (CNS) permeabilities. The *in silico* metabolism study includes the prediction of hits as inhibitors of CYP1A2, CYP2C19, CYP2C9, and CYP2D6. In addition, pkCSM also predicts hits as CYP2D6 and CYP3A4 substrates. Total clearance and renal organic cation transporter 2 (OCT2) are two criteria to evaluate the excretion of hits. In evaluating the safety profile of hits, we used pkCSM to predict AMES toxicity and hepatotoxicity. Moreover, we employed the web server to predict the potency of hits as hERG I and II inhibitors. We utilized a tidyverse package (Wickham *et al.*, 2019) in an R environment to assist with ADMET analysis.

MD simulations

MD simulations were performed to evaluate the binding energy of the selected compounds compared with the N3 and GC376 inhibitors. The ligand was deployed in the AMBER force field with GAFF (Wang *et al.*, 2004) and the 3CL^pro with ff14SB (Maier *et al.*, 2015). Each protein–ligand was solvated in a TIP3P water model as an explicit solvent with a minimum boundary distance of 10 Å. Also, the numbers of Na^+ and Cl^- ions were added to each protein–ligand complex to acquire the neutralization and physiological state. All systems were minimized, heated gradually to 310 K, and equilibrated, which eventually produced 100 ns trajectories. Afterward, binding energy values were computed from the last frame MD trajectory using molecular mechanics with a generalized born and surface area solvation (MMGBSA) method.

Visualization

Molecular interactions between the best hits, which have good ADMET profiles, and the binding site of 3CL^pro were visualized using BIOVIA DS 2020 Client. The generated images were processed further using GNU Image Manipulation Program 2.10.

RESULTS AND DISCUSSION

Molecular docking validation

As the validation step in the virtual screening campaign, we conducted a redocking procedure on the crystal structure of SARS-CoV-2 3CL^pro (hereafter mentioned as 3CL^pro) and its ligand (N3), which is deposited in the PDB as 6LU7. Such a procedure ensures that the stochastic search method reaches a global minimum (Forli *et al.*, 2016). We achieved a RMSD of less than 2 Å in the redocking procedure by applying grid box dimensions of 26 × 32 × 32 with 1 Å spacing. The best pose of N3 has a binding energy score of −10.14 kcal/mol in binding to 3CL^pro.

Virtual screening campaigns

In the next step, we performed a virtual screening campaign of 378 *Erythrina* flavonoids from *Erythrina* against 3CL^pro (Table S1). These flavonoids include 18 flavones, 3 flavonols, 91 flavanones, 14 chalcones, 11 isoflavans, 5 isoflav-3-enes, 43 isoflavanones, 99 isoflavones, 42 pterocarpans, 14 6α-hydroxypterocarpans, 7 pterocarpenes, 5 coumestans, 3 3-arylcoumarins, 1 coumaronochromone, 15 2-arylbenzofurans, 2 3-aryl-2,3-dihydrobenzofurans, and 1 biflavonoid. Every compound was subjected to a 50-run molecular docking, and the results are summarized in Table S1.

Of 378 *Erythrina* flavonoids, 108 possess binding energy scores stronger than that of N3 (−10.14 kcal/mol) (Table 1). Most of these flavonoids, having high binding affinities to 3CL^pro, belong to flavanones and isoflavones. Several 40 hits are flavanones with erycaffra F (57) as the strongest 3CL^pro binder within the group (−11.93 kcal/mol), while 34 others are isoflavones. The best hit from the isoflavone group is 6,8-diprenylorobol (211) with a binding energy score of −12.18 kcal/mol. Isoflavanones are the third largest group of flavonoids from *Erythrina* with binding energy scores stronger than that of N3. This flavonoid group shares 15 hits, where the most negative binding energy (−12.04 kcal/mol) is owned by orientanol E (171). The rest of the flavonoids with tight binding to 3CL^pro consist of five flavones, four isoflavans, two chalcones, two pterocarpans, two 6α-hydroxypterocarpans, one flavonol, one pterocarpene, and one biflavonoid. Meanwhile, none of the isoflav-3-enes, coumestans, 3-arylcoumarins, coumaronochromones, 2-arylbenzofurans, coumaronochromones, 2-arylbenzofurans, and 3-aryl-2,3-dihydrobenzofurans is stronger than N3 in binding to 3CL^pro.

The top hit among the flavonoid groups is kaempferol-3-O-(2″-O-β-D-glucopyranosyl-6″-O-α-L-rhamnopyranosyl-β-D-glucopyranoside) (20), a flavonol, with a binding energy score of −13.23 kcal/mol. The second top hit is a flavone, vicenin-2 (16), followed by 6,8-diprenylorobol (211) and vogelin H (277) which are isoflavones. The fifth top hit is orientanol E (171), belonging to isoflavanones.

The conducted virtual screening campaign suggests that many flavonoids from *Erythrina* are potential 3CL^pro inhibitors. Nonetheless, these compounds should fulfill drug-likeness criteria to be active as oral drugs. Therefore, in the next step, we assessed the resulting hits using Lipinski's Ro5 through the SwissADME web server.
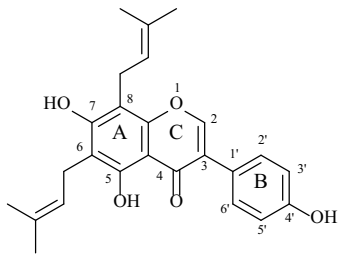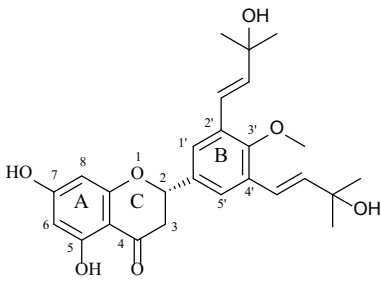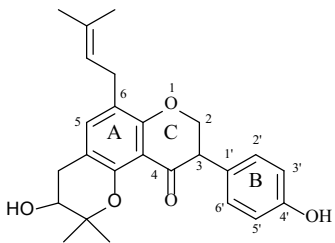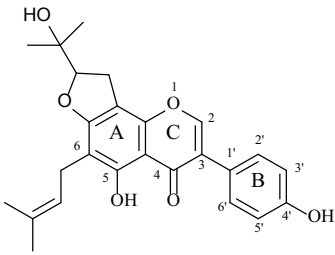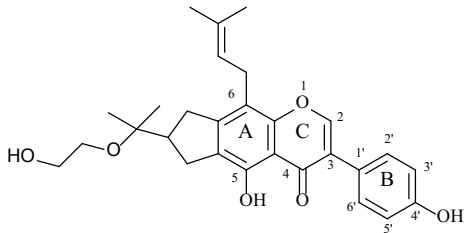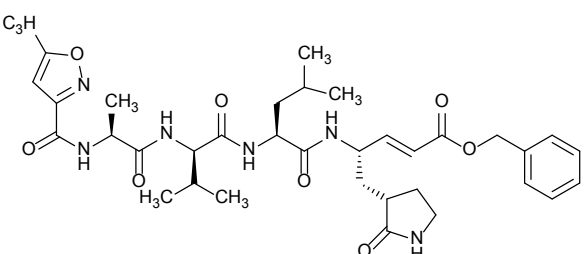
Lipinski's Ro5

Several of the 108 hits were further assessed for their drug-likeness using Lipinski's Ro5 through the SwissADME web server. According to Ro5, drugs should have a MW less than 500 Da, HBD and HBA less than 5 and 10, respectively, and logP less than 5. Compounds should fulfill three rules for the minimum requirement as drug-like molecules (Lipinski *et al.*, 2012; Raj, 2021).

The result of the Ro5 assessment suggested that only five hits failed to satisfy these three rules (Table S2). Three of them belong to flavones, namely, apigenin-7-O-rhamnosyl-6-C-glucoside (14), vicenin-1 (15), and vicenin-2 (16). The others are kaempferol-3-O-(2″-O-β-D-glucopyranosyl-6″-O-α-L-rhamnopyranosyl-β-D-glucopyranoside) (20) and auriculatin 4'-O-glucoside (189), which are a flavonol and an isoflavanone, respectively. Compounds (20) and (16) are the top first and second hits in the conducted virtual screening campaign, but they do not fulfill the minimum requirement for potential orally active drugs. This issue can be addressed by implementing synthetic carriers to improve the solubility, bioavailability, and stability of (20) and (16). For example, Uekama (1999) used cyclodextrin as the synthetic carrier, whereas Choudhury (2020), Du and Chen (2019), and Vyas *et al.* (2014) used a liposome. Various strategies can improve drug bioavailability, such as lipid nanoparticles or sugar moieties. A study demonstrated that the lipid group increased passive diffusion across epithelial barriers. Also, the

Table 1. Top 10 hits from virtual screening campaigns possessing binding energy values stronger than that of the N3 inhibitor.

Structure*	Classification	Name and Compound Number	Binding Energy (kcal/mol)
	Flavonol	Kaempferol-3-O-(2′-O-β-ᴅ-glucopyranosyl-6′-O-α-L-rhamnopyranosyl-β-ᴅ-glucopyranoside) (20)	−13.41
	Flavone	Vicenin-2 (16)	−12.74
	Isoflavone	6,8-Diprenylorobol (211)	12.18
	Isoflavone	Vogelin H (277)	−12.15
	Isoflavanone	Orientanol E (171)	−12.04

Continued

Structure*	Classification	Name and Compound Number	Binding Energy (kcal/mol)
	Isoflavone	6,8-Diprenylgenistein (206)	−11.97
	Flavanone	Erycaffra F (57)	−11.93
	Isoflavanone	Eryzerin B (168)	−11.93
	Isoflavone	Senegalensin (273)	−11.90
	Isoflavone	Eriotriochin (279)	−11.88
	Reference inhibitor	N-[(5-methylisoxazol-3-yl) carbonyl] alanyl-L-valyl-N-1-((1R, 2Z)-4-(benzyloxy)-4-oxo-1-{[(3R)-2-oxopyrrolidin-3-yl] methyl} but-2-enyl)-L-leucinamide (N3)	−10.14

*The numbering on 2D structures is only for rings A, B, and C of flavonoids.

polyhydroxylated nature of sugars provides increasing water solubility and facilitates transport across the BBB. Hence, some combinations may enhance the solubility and permeability of drugs (Blanchfield and Toth, 2004).

Most of the hits, 103 flavonoids, fulfill the minimum requirement of Ro5. Some 101 satisfy all the rules of Ro5, whereas vitexin (**11**) and bis-sigmodiol (**378**) violate the rule of HBA number (Table S2). These results suggest that those 103 flavonoids are drug-like molecules and potential orally active drug candidates.

In silico ADMET

Oral is the most popular route for drug administration due to its convenience for patients (Alqahtani *et al*., 2021). Through oral administration, drug molecules follow a journey including ADME. Therefore, 103 flavonoids satisfying Ro5 also should be further assessed according to their ADME criteria inside the body. Moreover, their toxicities should be evaluated to describe their safety profile. In this work, we utilized the pkCSM web server (http://biosig.unimelb.edu.au/pkcsm/), which offers more comprehensive feature predictions than SwissADME, to study the *in silico* absorption, metabolism, excretion, and toxicity.

In silico predictions to assess absorption criteria of 103 flavonoids include water solubility, human intestinal absorption, Caco2 permeability, P-glycoprotein substrate, and P-glycoprotein I and II inhibitors. Prediction results suggest that the 103 flavonoids have good water solubility and human intestinal absorption (Table S3), which are expected since they fulfill Ro5, as predicted by SwissADME. Nonetheless, only 69 flavonoids have good Caco2 permeabilities, with predicted values greater than 0.900. As one of the top hits, compound (**171**) has a predicted value of 0.771, which fails to satisfy Caco2 permeability. It is worth noting that the Caco2 permeability assay uses a cell line originating from a human colorectal carcinoma which represents the discrimination of drug absorption in the large intestine (Artursson and Karlsson, 1991). In terms of P-glycoprotein-related absorption, the pkCSM web server predicts the 103 flavonoids as P-glycoprotein substrates, implying that they are readily pumped back to the lumen, lowering their absorption. However, 85 of them are P-glycoprotein I inhibitors, 78 are P-glycoprotein II inhibitors, and 64 are inhibitors for both proteins. Compounds (**171**), (**211**), and (**277**), which are on the top hit list, are inhibitors for both P-glycoproteins I and II. Inhibition of P-glycoproteins I and II increase the bioavailability of molecules that are P-glycoprotein substrates (Finch and Pillans, 2014).

After absorption via the small intestine, drug molecules are distributed to their targets and tissues through the blood and lymphatic circulatory systems. Therefore, distribution is a vital pharmacokinetic parameter for monitoring the number of drug molecules reaching target cells (Twardowski and Ksiazek, 1983; Zhivkova *et al*., 2015). For the distribution aspect, pkCSM predicts the VDss, fraction unbound in humans, BBB permeability, and CNS permeability.

VDss represents the propensity of drug molecules to reside in the plasma or distribute in tissues. Drugs with higher VDss values are distributed more in tissue than in plasma, thus requiring greater doses, and vice versa. Only four flavonoids are predicted to have high values of distribution volumes (log VDss > 0.45). Some 24 flavonoids have low log VDss values below −0.15, including compound (**211**) as one of the top hits. The

values of log VDss for the other 75 flavonoids are between −0.15 and 0.45 (Table S4). Therefore, the majority of the flavonoids complying with Ro5 may be more distributed in plasma. However, all these flavonoids have high fractions of bound forms to proteins in the blood plasma, indicated by low values of predicted unbound states. These predictions may reflect the low bioavailability of the flavonoids and their inefficiency in diffusing the membrane cells. A study conducted by Vandyck and Deval (2021) suggests that the low bioavailability of 3CL^pro inhibitors can be addressed by injection or inhalation administration. Moreover, cyclodextrin delivery systems such as 2-hydroxypropyl-β-cyclodextrin (Glisoni *et al*., 2012; Jeulin *et al*., 2009; Nguyen and Van Den Mooter, 2014), randomly methylated β-cyclodextrin (Pathak *et al*., 2010), and α-cyclodextrin (αCD) are other solutions for the low bioavailability issue.

Another distribution criterion is BBB permeability. The BBB plays a key role in limiting the distribution of foreign molecules, which may be toxic, to the brain (Faria *et al*., 2012). BBB permeability can be expressed as logBB, which reflects the ability of drug molecules to enter the brain. None of the 103 hits are readily distributed to the brain (logBB > 0.3) and 45 of them poorly crossed the BBB (logBB < −1) (Table S4). However, the blood–barrier permeability surface product (logPS) prediction, which is derived from more direct measurement, suggests that 38 hits can easily enter the CNS, while 18 others are not permeable, such as compounds (**16**) and (**20**). A study conducted by Zanin *et al*. (2020) revealed that SARS-CoV-2 infects the brain. Therefore, those 38 hits potentially inhibit the virus's growth in the brain. Nevertheless, those hits should be free from mutagenesis and carcinogenesis properties (Gyebi *et al*., 2021).

The next step after drug distribution is metabolism or biotransformation. Metabolism may occur before or after drug molecules reach target cells. It is an essential process in activating drug molecules and inactivating target cells and the excretion system, respectively (Wilde *et al*., 2019). Cytochrome P450 or the CYP superfamily are groups of enzymes that highly participate in drug metabolism, with CYP2C, CYP2D, and CYP3A subfamilies as the most active (Tushar *et al*., 2007). The pkCSM web server provides a series of predictions for drug molecules or secondary metabolites likely to be substrates or inhibitors for such proteins. It predicts that none of the hits is a CYP2D6 substrate and 14 hits are CYP3A4 substrates. These 14 hits are potentially metabolized by CYP3A4, increasing their elimination rates and decreasing their bioavailabilities in the body. However, further metabolism prediction suggests that 10 of them are CYP3A4 inhibitors, along with the other 30 hits. Other cytochromes, CYP1A2 and CYP2C19, are potentially inhibited by 29 and 89 hits, respectively. Meanwhile, CYP2C9 may be inhibited by 90 hits (Table S5). Of all hits, compound (**259**) may inhibit five cytochromes, including CYP1A2, CYP2C19, CYP2C9, CYP2D6, and CYP3A4. Inhibition of one or more cytochromes can increase the bioavailability of other hits from *Erythrina* plants.

The last step in pharmacokinetics is excretion, which reduces the concentration of drug molecules at their active sites. Slow total clearance of drug molecules via renal or hepatic excretion assists in the maintenance of therapeutic effects. Total clearance affects the bioavailability and half-life of drug molecules, which determine their dose sizes and regimens. The pkCSM web server provides a total clearance prediction, in log(CLtot), representing a combination of renal and hepatic clearance. Some 10 hits are

classified as high total clearance with log(CLtot) more than 0.7. Those hits could be quickly cleared from the blood by the liver. Some 56 hits are intermediate total clearance, with log(CLtot) values between 0.3 and 0.7, whereas some 37 hits are low total clearance, with log(CLtot) less than 0.3 (Table S6). The other excretion parameter is the renal OCT2 substrate. OCT2 has a key role in the distribution and renal elimination of endogenous and drug molecules. Its substrates may have adverse interactions with OCT2 inhibitors. Therefore, predicting all hits as OCT2 substrates is beneficial for their potential contraindication and clearance (Pires *et al.*, 2015). Interestingly, pkCSM only predicts erysubin D (**329**) as an OCT2 substrate. This prediction indicates the safety profile of the majority of the flavonoids from *Erythrina* plants in terms of contraindication due to OCT2.

Drug candidates often fail in the late phases of development due to their toxicities. Therefore, a preliminary toxicity study through pkCSM would be beneficial. All 103 hits are not hERG I inhibitors, but 37 of them inhibit hERG II (Table S7). Inhibition of hERG causes heart rhythm abnormality, which may lead to fatal arrhythmia (Raschi *et al.*, 2009). Another toxicity parameter provided by pkCSM is AMES toxicity. The pkCSM web server predicts 96 hits are AMES-toxicity-free, while the other 7 have a positive result prediction (Table S7), suggesting their carcinogenicity potentials. For hepatoxicity prediction, 15 hits potentially damage the liver (Table S7). In total, pkCSM predicts 33 hits free from hepatoxicity and mutagenicity. Additionally, they are non-hERG I and II inhibitors. Two of them, orientanol E (**171**) and erycaffra F (**57**), are the fifth and seventh on the top hit list.

Non-bonded interactions analysis

Among 33 flavonoids that are considered hepatoxicity- and mutagenicity-free according to *in silico* ADMET above, orientanol E (**171**) and erycaffra F (**57**) are the fifth and seventh on the top hit list of virtual screening (Tables S1 and S7). Therefore, they are potential 3CL^pro inhibitor candidates, and their detailed interaction analysis with the enzyme is interesting to explore.

We performed interaction analysis for all poses of orientanol E (**171**) and erycaffra F (**57**) in their best clusters (Tables S8–S10). The results (Tables S8–S11) showed that both flavonoids interact with His41 and Cys145, dyad catalytic residues, which are important to 3CL^pro inhibition activity (Konwar and Sarma, 2021; Tahir Ul Qamar *et al.*, 2020). Orientanol E (**171**) forms a salt bridge with His41 through its C7-OH, which is predicted in a deprotonated state (Fig. 1). Such an interaction presents in all poses docked to the binding site of 3CL^pro. Furthermore, it also interacts with His41 via π-π T-shape stacking, where its occurrence is 80.5% in all poses in the best cluster. Meanwhile, erycaffra F (**57**) interacts with His41 solely through a π-alkyl with an occurrence of 92.1% in all poses (Tables S10 and S11). For Cys145, both flavonoids form a hydrophobic alkyl interaction which emerges in 90.2% and 81.6% among all poses of orientanol E (**171**) and erycaffra F (**57**), respectively.

Separate studies conducted by Cannalire *et al.* (2022) and Zhang *et al.* (2020) suggest that the interaction with His163 is essential for the inhibition of 3CL^pro, as demonstrated on baicalein. Orientanol E (**171**) and erycaffra F (**57**) also form interactions with His163 (Figs. 1 and 2). For erycaffra F (**57**), the interaction with this residue is through an H-bond, which appears in all poses (Tables S10 and S11). In the case of orientanol E (**171**), His163 makes a hydrophobic π-alkyl with almost all poses of the

flavanone (Tables S8 and S9). Additionally, orientanol E (**171**) forms a hydrophobic alkyl interaction with Met49. It is another vital residue for the inhibition of 3CL^pro, situated on the floor of the binding pocket. Xiang *et al.* (2022) suggested that the interaction with this residue hinders the native substrate from docking at the active site of 3CL^pro.

Orientanol E (**171**) also interacts with Met165 and Pro168 with an occurrence of more than 80% within poses in the best molecular docking hit cluster (Tables S8 and S9). Moreover, it builds interactions with some residues, including His41, Ala191, Arg188, Gln189, Leu167, Cys145, Gln192, Glu166, Met165, Thr190, Cys44, Pro52, His164, His172, and Tyr54. These interactions occur in 80% poses of the best hit cluster. Nonetheless, it has unfavorable interactions. For example, the best pose of orientanol E (**171**) exhibits such an unfavorable interaction with Glu166. Meanwhile, erycaffra F (**57**) interacts with Met165, Pro168, Arg188, Gln189, and Gln192, which almost exist in all poses (80% occurrence). Additionally, it interacts with the binding site of 3CL^pro without any unfavorable interaction. It also forms another interaction with Leu167, Pro168, Ala191, His172, Glu166, Arg188, His41, Ser144, Tyr54, Cys145, Gln192, Gln189, Gln192, Met49, Asp187, Thr190, Leu141, and Met49. However, the interactions do not occur in the majority of poses, with occurrence in less than 80%. Orientanol E (**171**) has seven types of nonbonded interactions, including attractive charge, conventional hydrogen bond, alkyl, π-alkyl, π-π T-shaped, π-sigma, and π-sulfur, whereas erycaffra F (**57**) forms six interaction categories (carbon-hydrogen bond, conventional hydrogen bond, alkyl, amide π-stacked, π-alkyl, and dan π-sigma). Overall, the number of interactions built by erycaffra F (**57**) is higher than that by orientanol E (**171**) (Table 2, Table S1). These nonbonded interactions may explain the more negative intermolecular energy of erycaffra F (**57**) than orientanol E (**171**), although the best pose of orientanol E (**171**) has more binding energy than that of erycaffra F (**57**).

Another binding energy component in molecular docking is torsional energy. *Isa et al.* (2022) and Kumar *et al.* (2020) showed that torsional bonds maintain ligand flexibility in the rigid binding site of 3CL^pro. According to molecular docking analysis, orientanol E (**171**) has lower torsional energy than erycaffra F (**57**) (Table 4), which is in agreement with their binding energy values. The torsional energy values suggest that orientanol E (**171**) may have a higher potency than erycaffra F (**57**) in binding to the active site of 3CL^pro due to its flexibility.

MD simulations

Molecular docking is widely used in structural-based virtual screening due to its rapid evaluation, which was implemented in this study to screen flavonoids in the genus *Erythrina* against 3CL^pro. However, it suffers several limitations, such as employing a rigid receptor and simplifying a scoring function (Forli *et al.*, 2016). Forli *et al.* (2016) recommended MD simulation method to refine the top hits obtained from molecular docking; MD also mimics a physiological condition which helps to estimate the strength of binding energy between the ligand and the target protein as an experimental study (Kumar *et al.*, 2020). Therefore, we subjected 3CL^pro-bound orientanol E (**171**) and erycaffra F (**57**) to MD simulations, yielding a 100 ns trajectory for each complex.

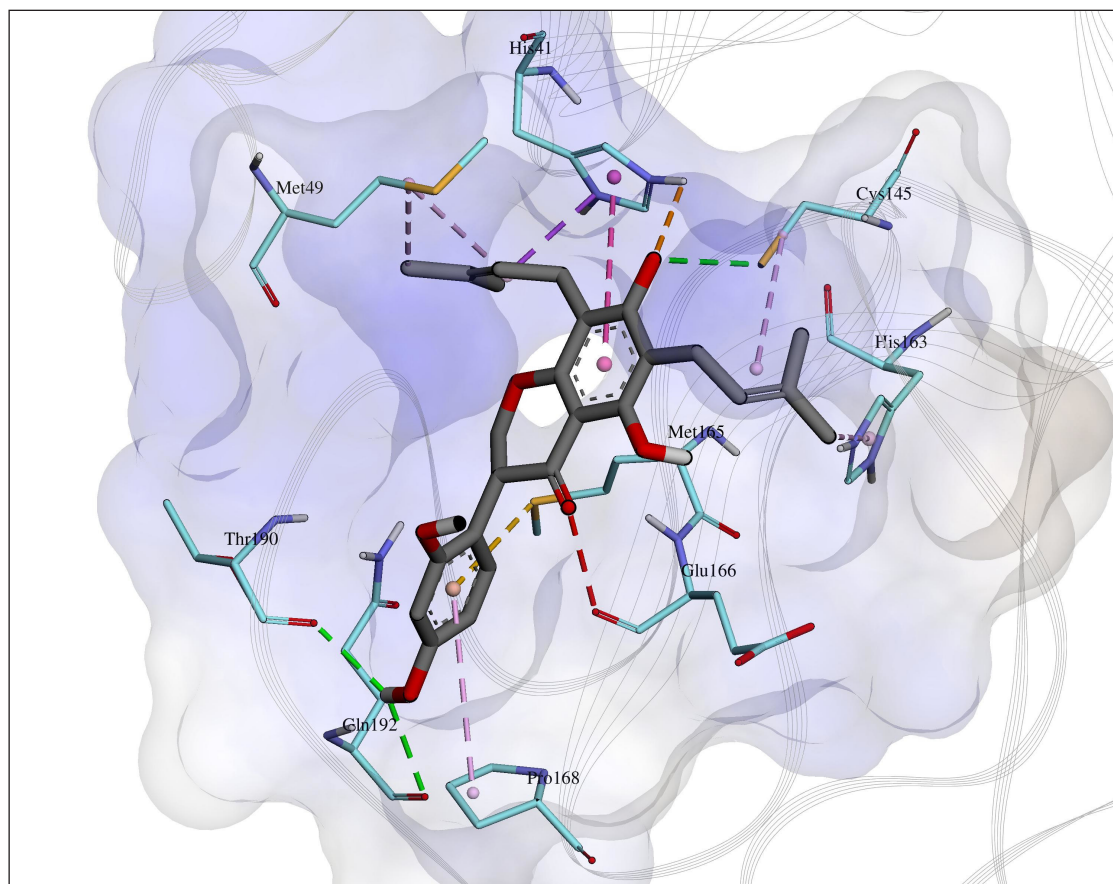Additionally, we conducted MD simulations on the 3CL^pro-bound N3 and GC376 as the references. N3 is a potent

Figure 1. The visualization of interactions between orientanol E (171) and 3CLpro. The carbon atoms for the residues on the binding site of 3CLpro are in a light-blue color, whereas those for orientanol E (171) are in grey. The orange dash line depicts the interaction of pi anion and attractive charge, the green for hydrogen bond, the purple, and pink for hydrophobic interactions including alkyl, amide-π stacked, π-alkyl, π-π T-shaped, and π-sigma. Meanwhile, the yellow dash line denotes the interaction of π-sulfur, whereas the red for unfavorable interaction.
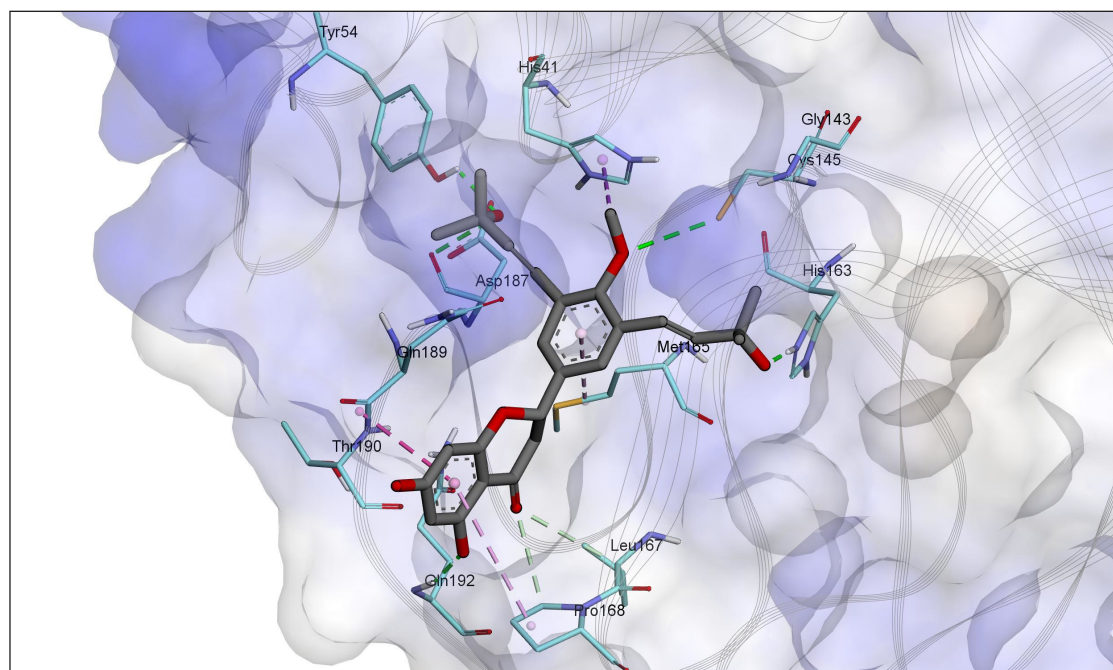

Figure 2. Visualization of interactions between erycaffra F (57) and 3CLpro. The carbon atoms for the residues on the binding site of 3CLpro are in a light-blue color, whereas those for orientanol E (171) are in grey. The orange dash line depicts the interaction of π-anion, the green for hydrogen bond, the light green for carbon hydrogen interaction, the purple and pink for hydrophobic interactions including alkyl, amide-π stacked, π-alkyl, π-π T-shaped, and π-sigma. Meanwhile, the yellow dash line denotes the interaction of π-sulfur, whereas the red for unfavorable interaction.

Table 2. Non-bonded interaction types between the binding site of 3CL^{pro} and two flavonoids, orientanol E (**171**), and eryvsffra F (**57**). These flavonoids have good ADMET profiles and are in the top 10 hits.

Interaction	Orientanol E (171)	Erycaffra F (57)
Salt bridge (attractive charge)	1	-
Carbon H-bond	-	2
Conventional H-bond	3	5
Alkyl	2	5
Amide π-Stacked	-	1
π-Alkyl	2	4
π-π T-shaped	1	-
π-Sigma	1	1
π-Sulfur	1	-
Unfavorable	1	-

Table 3. Binding energy values between 3CL^{pro} and ligands obtained from MD simulation. The ligands are orientanol E (**171**), erycaffra F (**57**), N3, GC376, and paxlovid. Binding energy values from MD simulations were computed using a MMGBSA method.

Components	Binding energy
	MD simulation
N3	−58.11 kcal/mol
GC376	−20.25 kcal/mol
Paxlovid	−42.23 kcal/mol
Orientanol E (**171**)	−35.47 kcal/mol
Erycaffra (**57**)	−20.06 kcal/mol

SARS-CoV-2 3CL^{pro} inhibitor, which can also inhibit multiple coronaviruses, like MERS-CoV and SARS-CoV (Jin *et al.*, 2020). Meanwhile, GC376 has been widely investigated as a potential inhibitor targeting 3CL^{pro} in Vero cells against FCoV, SARS-CoV, MERS-CoV, and SARS-CoV-2 (Fu *et al.*, 2020; Sharun *et al.*, 2021). It is also employed as a standard inhibitor in a commercial 3CL^{pro} assay kit (BPS Bioscience, 2022). Hence, the utilization of N3 and GC376 as the references assists in predicting the inhibition potential of orientanol E (**171**) and erycaffra F (**57**) to 3CL^{pro}.

Binding energy evaluations from MD simulations are tabulated in Table 3. The binding energy values change from molecular docking. These changes may be due to MD simulations accommodating complete flexibility in both ligands and 3CL^{pro}, allowing intermolecular interaction adjustment (Hardianto *et al.*, 2017, 2019) between them (Table S12). Based on MD simulation, N3 and Paxlovid bind 3CL^{pro} stronger than orientanol E (**171**) and erycaffra F (**57**). Nevertheless, orientanol E (**171**) still has a more negative binding energy value (−35.47 kcal/mol) than GC376 (−20.25 kcal/mol), which is comparable to that of erycaffra F (**57**) (−20.06 kcal/mol). These results suggest that both orientanol E (**171**) and erycaffra F (**57**) are potential 3CL^{pro} inhibitors.

CONCLUSION

In this study, we have performed structure-based virtual screening campaigns on 378 flavonoids from the genus *Erythrina*

against SARS-CoV-2 3CL^{pro}. These virtual screening campaigns filtered 108 hits with binding energy scores stronger than the N3 inhibitor. Some 103 of the hits satisfy Lipinski's Ro5, suggesting their potency as oral drug candidates. Additionally, we conducted an *in silico* ADMET study using the pkCSM web server on the 108 hits since ADME and safety profiles of molecules are essential in drug discovery and development. The web server suggests that 33 flavonoids are hepatotoxicity- and mutagenicity-free. In addition, they are not hERG I and II inhibitors. Two of them, orientanol E (**171**) and erycaffra F (**57**), have binding energy values in the top 10 hits. Binding energy evaluation from MD simulation also supports both orientanol E (**171**) and erycaffra F (**57**) as potential 3CL^{pro} inhibitors. Both flavonoids satisfy Ro5 and have good absorption profiles, but their distribution properties are poor according to pkCSM prediction. These issues can be anticipated using delivery systems such as liposome and cyclodextrin. The pkCSM web server predicts both flavonoids as nonsubstrates for CYP2D6 and CYP3A4, suggesting their high bioavailability in the body. According to the web server, they may be cleared from the body through feces. In summary, this study suggests that flavonoids from *Erythrina* may have the potency to be developed as herbal medicines to treat COVID-19 through inhibition of 3CL^{pro}. Further *in vitro* and *in vivo* experiments, however, are required to confirm this notion.

CONFLICTS OF INTEREST

All authors declare that they have no conflicts of interest.

AUTHORS' CONTRIBUTIONS

All authors made substantial contributions to conception and design, acquisition of data, or analysis and interpretation of data; took part in drafting the article or revising it critically for important intellectual content; agreed to submit to the current journal; gave final approval of the version to be published; and agreed to be accountable for all aspects of the work. All the authors are eligible to be an author as per the International Committee of Medical Journal Editors (ICMJE) requirements/guidelines.

ETHICAL APPROVALS

This study does not involve experiments on animals or human subjects.

DATA AVAILABILITY

All data generated and analyzed are included within this research article.

PUBLISHER'S NOTE

This journal remains neutral with regard to jurisdictional claims in published institutional affiliation.

REFERENCES

Ahmad B, Batool M, Ain QU, Kim MS, Choi S. Exploring the binding mechanism of PF-07321332 SARS-CoV-2 protease inhibitor through molecular dynamics and binding free energy simulations. Int J Mol Sci, 2021; 22:17.

Alqahtani MS, Kazi M, Alsenaidy MA, Ahmad MZ. Advances in oral drug delivery. J Front Pharmacol, 2021; 12:618411.

Artursson P, Karlsson J. Correlation between oral drug absorption in humans and apparent drug permeability coefficients in human intestinal epithelial (Caco-2) cells. J Biochem Biophys Res Commun, 1991; 175(3):880–5.

Blanchfield J, Toth I. Lipid, sugar, and liposaccharide based delivery systems 2. Curr Med Chem, 2004; 11:2375–82.

BPS Bioscience. 3CL protease, untagged (SARS-CoV-2) assay kit. BPS Bioscience, Inc., 2022. [Online] Available via https://bpsbioscience.com/3cl-protease-untagged-sars-cov-2-assay-kit-78042 (Accessed 23 March 2022).

Cannalire R, Cerchia C, Beccari AR, Di Leva FS, Summa V. Targeting SARS-CoV-2 proteases and polymerase for COVID-19 treatment: state of the art and future opportunities. J Med Chem, 2022; 65(4):2716–46.

ChemAxon. Marvin sketch 20.11.0 software. 2020. [Online] Available via http://www.chemaxon.com (Accessed 11 February 2020).

Cheng F, Li W, Zhou Y, Shen J, Wu Z, Liu G, Lee PW, Tang Y. AdmetSAR: a comprehensive source and free tool for assessment of chemical ADMET properties. J Chem Inf Model, 2012; 52(11):3099–105.

Choudhury A. Liposome: a carrier for effective drug delivery. J App Pharm Res, 2020; 8(1):22–8.

Cui J, Li F, Shi ZL. Origin and evolution of pathogenic Coronaviruses. J Nat Rev Microbiol, 2019; 17(3):181–92.

Daina A, Michielin O, Zoete V. SwissADME: a free web tool to evaluate pharmacokinetics, drug-likeness and medicinal chemistry friendliness of small molecules. J Sci Rep, 2017; 7(1):42717.

Du Y, Chen B. Combination of drugs and carriers in drug delivery technology and its development. J Drug Des Devel Ther, 2019; 13:1401–8.

Fahmy NM, Al-Sayed E, El-Shazly M, Singab AN. Comprehensive review on flavonoids biological activities of *Erythrina* plant species. J Ind Crops Prod, 2018; 123:500–38.

Fahmy NM, Al-Sayed E, Moghannem S, Azam F, El-Shazly M, Singab AN. Breaking down the barriers to a natural antiviral agent: antiviral activity and molecular docking of *Erythrina* speciosa extract, fractions, and the major compound. J Chem Biodivers, 2020; 17(2):e1900511.

Faria A, Mateus N, Calhau C. Flavonoid transport across blood-brain barrier: implication for their direct neuroprotective actions. J Nutr Aging, 2012; 1(2):89–97.

Finch A, Pillans P. P-glycoprotein and its role in drug-drug interactions. J Aust Prescr, 2014; 37(4):137–9.

Forli S, Huey R, Pique ME, Sanner M, Goodsell DS, Arthur J. Computational protein-ligand docking and virtual drug screening with the AutoDock suite. J Nat Protoc, 2016; 11(5):905–19.

Fu L, Ye F, Feng Y, Yu F, Wang Q, Wu Y, Zhao C, Sun H, Huang B, Niu P, Song H, Shi Y, Li X, Tan W, Qi J, Gao GF. Both Boceprevir and GC376 efficaciously inhibit SARS-CoV-2 by targeting its main protease. Nat Commun, 2020; 11(1):1–8.

Gil C, Ginex T, Maestro I, Nozal V, Barrado-Gil L, Cuesta-Geijo MÁ, Urquiza J, Ramírez D, Alonso C, Campillo NE, Martinez A. COVID-19: drug targets and potential treatments. J Med Chem, 2020; 63(21):12359–86.

Glisoni RJ, Cuestas ML, Mathet VL, Oubiña JR, Moglioni AG, Sosnik A. Antiviral activity against the hepatitis C virus (HCV) of 1-indanone thiosemicarbazones and their inclusion complexes with hydroxypropyl-β- cyclodextrin. Eur J Pharm Sci, 2012; 47(3):596–603.

Gohlke H, Hendlich M, Klebe G. Knowledge-based scoring function to predict protein-ligand interactions. J Mol Biol, 2000; 295(2):337–56.

Gyebi GA, Ogunyemi OM, Ibrahim IM, Ogunro OB, Adegunloye AP, Afolabi SO. SARS-CoV-2 host cell entry: an *in silico* investigation of potential inhibitory roles of terpenoids. J Genet Eng Biotechnol, 2021; 19(1):113.

Hardianto A, Khanna V, Liu F, Ranganathan S. Diverse dynamics features of novel protein kinase C (PKC) isozymes determine the selectivity of a fluorinated balanol analogue for PKCε. BMC Bioinform, 2019; 19(13):342.

Hardianto A, Yusuf M, Hidayat IW, Ishmayana S, Soedjanaatmadja UMS. Exploring the potency of nigella sativa seed in inhibiting sars-cov-2 main protease using molecular docking and molecular dynamics simulations. Indones J Chem, 2021; 21(5):1252–62.

Hardianto A, Yusuf M, Liu F, Ranganathan S. Exploration of charge states of balanol analogues acting as ATP-competitive inhibitors in kinases. BMC Bioinform, 2017; 18(16):572.

Herlina T, Nurlelasari, Kurnia D, Supratman U, Udin Z. *In vitro* anticancer and antimalarial Erystagallin-A from *Erythrina* variegata (L.) stem bark. Med Plants Int J Phytomed Relat Ind, 2011; 3(1):9–13.

Isa MA, Mustapha A, Qazi S, Raza K, Allamin IA, Ibrahim MM, Mohammed MM. *In silico* molecular docking and molecular dynamic simulation of potential inhibitors of 3C-like main proteinase (3CLpro) from severe acute respiratory syndrome coronavirus-2 (SARS-CoV-2) using selected african medicinal plants. J Adv Trad Med, 2022; 22(1):107–23.

Jeulin H, Venard V, Carapito D, Finance C, Kedzierewicz F. Effective ribavirin concentration in mice brain using cyclodextrin as a drug carrier: evaluation in a measles encephalitis model. J Antivir Res, 2009; 81(3):261–6.

Ji W, Wang W, Zhao X, Zai J, Li X. Cross-species transmission of the newly identified coronavirus 2019-nCoV. J Med Virol, 2020; 92(4):433–40.

Jin Z, Du X, Xu Y, Deng Y, Liu M, Zhao Y, Zhang B, Li X, Zhang L, Peng C, Duan Y, Yu J, Wang L, Yang K, Liu F, Jiang R, Yang X, You T, Liu X, Yang H. Structure of Mpro from SARS-CoV-2 and discovery of its inhibitors. J Nat, 2020; 582(7811):289–93.

Kavaliauskas P, Grybaite B, Mickevicius V, Petraitiene R, Grigaleviciute R, Planciuniene R, Gialanella P, Pockevicius A, Petraitis V. Synthesis, ADMET properties, and *in vitro* antimicrobial and antibiofilm activity of 5-nitro-2-thiophenecarbaldehyde N-((E)-(5-nitrothienyl) methylidene)hydrazone (KTU-286) against staphylococcus aureus with defined resistance mechanisms. J Antibiot, 2020; 9(9):1–17.

Kiemer L, Lund O, Brunak S, Blom N. Coronavirus 3CLpro proteinase cleavage sites: possible relevance to SARS virus pathology. BMC Bioinform, 2004; 5:1–9.

Kissler S, Tedijanto C, Goldstein E, Grad Y, Lipsitch M. Projecting the transmission dynamics of SARS-CoV-2 through the postpandemic period. J Sci, 2020; 368(6493):860–8.

Konwar M, Sarma D. Advances in developing small molecule SARS 3CLpro inhibitors as potential remedy for corona virus infection. J Tetrahedron, 2021; 77:131761.

Kumar S, Sharma PP, Shankar U, Kumar D, Joshi SK, Pena L, Durvasula R, Kumar A, Kempaiah P, Poonam, Rathi B. Discovery of new hydroxyethylamine analogs against 3CLpro protein target of SARS-CoV-2: molecular docking, molecular dynamics simulation, and structure-activity relationship studies. J Chem Inf Model, 2020; 60(12):5754–70.

Lee JS, Won KO, Jong SA, Yong HK, Mbafor JT, Wandji J, Fomum ZT. Prenylisoflavonoids from *Erythrina* senegalensis as novel HIV-1 protease inhibitors. J Planta Med, 2009; 75(3):268–70.

Lee J, Worrall LJ, Vuckovic M, Rosell FI, Gentile F, Ton AT, Caveney NA, Ban F, Cherkasov A, Paetzel M, Strynadka, NCJ. Crystallographic structure of wild-type SARS-CoV-2 main protease acyl-enzyme intermediate with physiological C-terminal autoprocessing site. J Nat Commun, 2020; 11(1):5877.

Lipinski CA, Lombardo F, Dominy BW, Feeney PJ. Experimental and computational approaches to estimate solubility and permeability in drug discovery and development settings. J Adv Drug Deliv Rev, 2012; 64:4–17.

Liu AL, Wang HD, Lee SM, Wang YT, Du GH. Structure–activity relationship of flavonoids as influenza virus neuraminidase inhibitors and their *in vitro* anti-viral activities. J Bioorg Med Chem, 2008; 16(15):7141–7.

Liu H, Ye F, Sun Q, Liang H, Li C, Li S, Lu R, Huang B, Tan W, Lai L. Scutellaria baicalensis extract and baicalein inhibit replication of SARS-CoV-2 and its 3C-like protease *in vitro*. J Enzyme Inhib Med Chem, 2021; 36(1):497–503.

Maier JA, Martinez C, Kasavajhala K, Wickstrom L, Hauser KE, Simmerling C. ff14SB: improving the accuracy of protein side chain and backbone parameters from ff99SB. J Chem Theory Comput, 2015; 11(8):3696–713.

Mody V, Ho J, Wills S, Mawri A, Lawson L, Ebert MCCJC, Fortin GM., Rayalam S. Taval S. Identification of 3-chymotrypsin like protease (3CLᵖʳᵒ) inhibitors as potential anti-SARS-CoV-2 agents. J Commun Biol, 2021; 4(1):93.

Morse JS, Lalonde T, Xu S, Liu WR. Learning from the past: possible urgent prevention and treatment options for severe acute respiratory infections caused by 2019-nCoV. J Chem Bio Chem, 2020; 21(5):730–8.

Nguyen DN, Van den Mooter G. The fate of ritonavir in the presence of darunavir. Int J Pharm, 2014; 475(1):214–26.

Pathak SM, Musmade P, Dengle S, Karthik A, Bhat K, Udupa N. Enhanced oral absorption of saquinavir with Methyl-Beta-Cyclodextrin-preparation *in vitro* and *in vivo* evaluation. Eur J Pharm Sci, 2010; 41(3–4):440–51.

Petrou A, Zagaliotis P, Theodoroula NF, Mystridis GA, Vizirianakis IS, Walsh TJ, Geronikaki A. Thiazole/thiadiazole/benzothiazole based thiazolidin-4-one derivatives as potential inhibitors of main protease of SARS-CoV-2. J Molecules, 2022; 27(7):2180.

Pires DEV, Blundell TL, Ascher DB. pkCSM: predicting small-molecule pharmacokinetic and toxicity properties using graph-based signatures. J Med Chem, 2015; 58(9):4066–72.

Prescott L. SARS-CoV-2 3CLᵖʳᵒ whole human proteome cleavage prediction and enrichment/depletion analysis. Comput Biol Chem, 2022; 98:107671.

Qamar MT, Ashfaq UA, Tusleem K, Mumtaz A, Tariq Q, Goheer A, Ahmed B. *In silico* identification and evaluation of plant flavonoids as dengue NS2B/NS3 protease inhibitors using molecular docking and simulation approach. Pak J Pharm Sci, 2017; 30(6):2119–37.

Raj R. Analysis of non-structural proteins, NSPs of SARS-CoV-2 as targets for computational drug designing. J Biochem Biophys Rep, 2021; 25:100847.

Ramírez D, Caballero J. Is it reliable to take the molecular docking top scoring position as the best solution without considering available structural data. J Molecules, 2018; 23(5):1–17.

Raschi E, Ceccarini L, De Ponti F, Recanatini M. HERG-related drug toxicity and models for predicting hERG liability and QT prolongation. J Expert Opin Drug Metab Toxicol, 2009; 5(9):1005–21.

Saur IML, Panstruga R, Schulze-Lefert P. NOD-like receptor-mediated plant immunity: from structure to cell death. Nat Rev Immunol, 2021; 21(5):305–18.

Sharun K, Tiwari R, Dhama K. Protease inhibitor GC376 for COVID-19: lessons learned from feline infectious peritonitis. Ann Med Surg, 2021; 61:122–5.

Su H, Yao S, Zhao W, Zhang Y, Liu J, Shao Q, Wang Q, Li M, Xie H, Shang W, Ke C, Feng L, Jiang X, Shen J, Xiao G, Jiang H, Zhang L, Ye Y, Xu Y. Identification of pyrogallol as a warhead in design of covalent inhibitors for the SARS-CoV-2 3CL protease. J Nat Commun, 2021; 12(1):1–12.

Tahir Ul Qamar M, Alqahtani SM, Alamri MA, Chen LL. Structural basis of SARS-CoV-2 3CLᵖʳᵒ and anti-COVID-19 drug discovery from medicinal plants. J Pharm Anal, 2020; 10(4):313–9.

Tushar T, Vinod T, Rajan S, Shashindran C, Adithan C. Effect of honey on CYP3A4, CYP2D6 and CYP2C19 enzyme activity in healthy human volunteers. J Basic Clin Pharmacol Toxicol, 2007; 100(4):269–72.

Twardowski Z, Ksiazek A. Pharmacokinetics in renal failure. J Pol Arch Med Wewn, 1983; 65(6):491–500.

Uekama K. Cyclodextrins in drug delivery system. J Adv Drug Deliv Rev, 1999; 36(1):1–2.

Vandyck K, Deval J. Considerations for the discovery and development of 3-chymotrypsin-like cysteine protease inhibitors targeting SARS-CoV-2 infection. J Virol, 2020; 49:36–40.

Vyas A, Kumar AS, Gidwani B. Carrier-based drug delivery system for treatment of acne. Sci World J, 2014; 2014(276260):1–14.

Wang J, Wolf RM, Caldwell JW, Kollman PA, Case DA. Development and testing of a general amber force field. J Comput Chem, 2004; 25(9):1157–74.

Wickham H, Averick M, Bryan J, Chang W, McGowan L, François R, Grolemund G, Hayes A, Henry L, Hester J, Kuhn M, Pedersen T, Miller E, Bache S, Müller K, Ooms J, Robinson D, Seidel D, Spinu, V, Yutani H. Welcome to the Tidyverse. J Open Source Softw, 2019; 4(43):1686.

Wilde M, Pichini S, Pacifici R, Tagliabracci A, Busardò FP, Auwärter V, Solimini R. Metabolic pathways and potencies of new fentanyl analogs. J Front in Pharmacol, 2019; 10:238.

Worldometers. Coronavirus cases. 2022. [Online] Available via https://www.worldometers.info/coronavirus/ (Accessed 14 July 2022).

Xiang R, Yu Z, Wang Y, Wang L, Huo S, Li Y, Liang R, Hao Q, Ying T, Gao Y, Yu F, Jiang S. Recent advances in developing small-molecule inhibitors against SARS-CoV-2. J Acta Pharm Sin B, 2022; 12(4):1591–623.

Yamamoto KZ, Yasuo N, Sekijima M. Screening for inhibitors of main protease in SARS-CoV-2: *in silico* and *in vitro* approach avoiding peptidyl secondary amides. J Chem Inf Model, 2022; 62(2):350–8.

Yang H, Xie W, Xue X, Yang K, Ma J, Liang W, Zhao Q, Zhou Z. Design of wide-spectrum inhibitors targeting coronavirus main proteases. PLoS Biol, 2005; 3(10):e324.

Zanin L, Saraceno G Panciani PP, Renisi G, Signorini L, Migliorati K, Fontanella MM. SARS-CoV-2 can induce brain and spine demyelinating lesions. J Acta Neurochir, 2020; 162(7):1491–4.

Zhang L, Lin D, Sun X, Curth U, Drosten C, Sauerhering L, Becker S, Rox K, Hilgenfeld R. Crystal structure of SARS-CoV-2 main protease provides a basis for design of improved a-ketoamide inhibitors, (PDB ID 6Y2F). J Sci, 2020; 368(6489):409–12.

Zhivkova Z, Mandova T, Doytchinova I. Quantitative structure – pharmacokinetics relationships analysis of basic drugs: volume of distribution. J Pharm Pharm Sci, 2015; 18(3):515–27.

Zhu J, Zhang H, Lin Q, Lyu J, Lu L, Chen H, Zhang X, Zhang Y, Chen K. Progress on SARS-CoV-2 3CLᵖʳᵒ inhibitors: inspiration from SARS-CoV 3CLᵖʳᵒ peptidomimetics and small-molecule anti-inflammatory compounds. J Drug Des Devel Ther, 2022; 16:1067–82.

SUPPLEMENTARY MATERIAL

Supplementary data can be downloaded from the journal's website